PX912 Fluid Coursework Project

P. H. D. Student, u2157194

1 Introduction

Slip at a solid boundary may arise from several distinct mechanisms. Molecular slip refers to incomplete momentum transfer between liquid and solid molecules at the interface and is fundamentally a nanoscale effect. Apparent slip emerges at the macroscale due to surface roughness, heterogeneity, or the presence of low viscosity layers, even when local no-slip conditions are satisfied. In continuum models, these effects are collectively represented through an effective slip length, which encapsulates both molecular and apparent slip mechanisms within a single boundary condition [1].

Slip effects become particularly important in micro and nanoscale flows, where surface to volume ratios amplify the influence of boundary conditions and can lead to substantial deviations from classical no clip predictions. Such effects have been implicated in enhanced transport in confined geometries and are of practical relevance in applications ranging from microfluidic devices to flow through carbon nanotubes [2].

For Newtonian fluids, the introduction of molecular slip at a solid boundary provides a means of regularising the unphysical stress singularities that arise at moving contact lines under a strict no slip condition. This motivates the use of Navier type slip boundary conditions, which relate the tangential velocity at the wall to the local shear rate. In this work, such boundary conditions are applied to pressure driven channel and pipe flows, allowing the influence of slip on velocity profiles and volumetric flux to be quantified within a controlled and analytically tractable setting.

Pressure driven channel and pipe flows provide canonical test cases for investigating slip effects, as they admit exact analytical solutions under both no slip and Navier

slip boundary conditions. These geometries therefore offer a controlled framework for validating numerical schemes and isolating the influence of boundary conditions on both local flow structure and global transport properties.

The aim of this report is to validate finite difference solvers for pressure driven Stokes flow against known analytical solutions, and to use these solvers to quantify the effect of Navier slip on velocity profiles and volumetric flux in channel and pipe geometries. The role of slip length is examined systematically, and the implications for flow enhancement relative to the classical no slip case are discussed. Where appropriate, the framework is extended to derive a shear dependent slip boundary condition for pipe flow [3], illustrating the onset of non-linear slip behaviour.

2 Computational Approach

2.1 Steady Poiseuille flow between two plates

Here we consider the steady viscous plane shear flow, subject to a constant applied pressure gradient G. In this case, the motion is plane parallel, with a velocity field that has a fixed direction with no variation along the direction of the flow

$$\mathbf{u} = (u(y), 0, 0). \tag{1}$$

The incompressibility condition is automatically satisfied since $\nabla \cdot \mathbf{u} = 0$. Furthermore, the non linear term in the Navier-Stokes equation $(\mathbf{u} \cdot \nabla)\mathbf{u}$ also vanishes. As a result, the governing equations reduce to a second order ODE for the velocity profile,

$$-\nu \frac{\partial^2 u}{\partial y^2} = G. \tag{2}$$

Where the viscosity ν is constant, and no-slip boundary conditions are enforced at the walls $u(\pm W) = 0$.

The governing equation can be solved analytically by integrating twice with respect to y and applying the no slip boundary conditions. This yields the Poiseuille velocity profile

$$\boxed{u(y) = \frac{G}{2\nu}\left(W^2 - y^2\right).} \tag{3}$$

This solution will be used to validate the numerical scheme in the following sections.

2.1.1 Finite difference discretisation

To compute the velocity profile numerically, discretise the domain $y \in [-W, W]$ using a uniform grid with n points,

$$y_i = -W + (i-1)h, \qquad i = 1, \ldots, n, \qquad h = \frac{2W}{n-1}. \tag{4}$$

Define the discrete approximation to the velocity by $u_i \approx u(y_i)$. At interior grid points, the second derivative is approximated using a second order centred finite difference,

$$\left.\frac{\mathrm{d}^2 u}{\mathrm{d}y^2}\right|_{y=y_i} \approx \frac{u_{i-1} - 2u_i + u_{i+1}}{h^2}, \qquad i = 2, \ldots, n-1. \tag{5}$$

Substituting into the governing equation gives the linear system

$$-\nu \frac{u_{i-1} - 2u_i + u_{i+1}}{h^2} = G, \qquad i = 2, \ldots, n-1, \tag{6}$$

or equivalently

$$-u_{i-1} + 2u_i - u_{i+1} = \frac{Gh^2}{\nu}, \qquad i = 2, \ldots, n-1. \tag{7}$$

The no slip boundary conditions are imposed directly at the endpoints,

$$u_0 = 0, \qquad u_n = 0. \tag{8}$$

This results in a tridiagonal system for the interior unknowns $\{u_i\}_{i=2}^{n-1}$, which is solved using a standard linear solver. The resulting numerical solution is then compared with the analytical Poiseuille profile to validate the method.

2.2 3D axisymmetric Poiseuille pipe flow

Consider now the steady, pressure driven flow in a straight circular pipe of radius R. In this case, the natural coordinate system to consider is cylindrical coordinates (r, θ, z), with the z-coordinate along the centre-line of the pipe and the boundary located at a constant radius $r = R$. Assuming that the velocity takes the form $\mathbf{u} = v_z(r)\mathbf{e}_z$, and we are ignoring the presence of gravity, the Navier-Stokes equation reduces to,

$$0 = -\frac{1}{\rho}\frac{\partial p}{\partial z} + \nu \frac{1}{r}\frac{\partial}{\partial r}\left(r\frac{\partial v_z}{\partial r}\right). \tag{9}$$

Assuming a constant pressure gradient G, the governing equation becomes,

$$\frac{1}{r}\frac{d}{dr}\left(r\frac{dv_z}{dr}\right) = -\frac{G}{\nu}. \tag{10}$$

Multiply through by r, integrate once and divide by r to obtain,

$$\frac{dv_z}{dr} = -\frac{G}{2\nu}r + \frac{C_1}{r}. \tag{11}$$

To avoid a singularity at $r = 0$, we must have $C_1 = 0$. Integrating again gives,

$$v_z(r) = -\frac{G}{4\nu}r^2 + C_2. \tag{12}$$

Finally, apply the no slip boundary condition $v_z(R) = 0$ to determine the constant C_2,

$$0 = -\frac{G}{4\nu}R^2 + C_2 \quad \Rightarrow \quad C_2 = \frac{G}{4\nu}R^2. \tag{13}$$

Therefore, the analytical result for 3D axisymmetric Poiseuille pipe flow is

$$\boxed{v_z(r) = \frac{G}{4\nu}(R^2 - r^2).} \tag{14}$$

2.2.1 Volume flux

The analytical volumetric flow rate is defined,

$$Q = \int_0^{2\pi} \int_0^R v_z(r) r \, dr \, d\theta. \tag{15}$$

Substituting the analytical radial velocity $v_z(r)$ yields,

$$Q = 2\pi \int_0^R \frac{G}{4\nu}(R^2 - r^2) r \, dr = \frac{\pi G R^4}{8\nu}. \tag{16}$$

This result shows that the volumetric flow rate scales as $Q \propto R^4$.

2.2.2 Finite discretisation

To compute the velocity profile for axisymmetric pipe flow, the radial domain $r \in [0, R]$ is discretised using a uniform grid with n points,

$$r_i = (i-1)h, \qquad i - 1, \ldots, n, \qquad h = \frac{R}{n-1}, \tag{17}$$

where $u_i \approx u(r_i)$ denotes the discrete velocity.

The governing equation,

$$\frac{1}{r}\frac{\mathrm{d}}{\mathrm{d}r}(r\frac{\mathrm{d}v_z}{\mathrm{d}r}) = -\frac{G}{\nu}, \tag{18}$$

is discretised at interior grid points using a second order conservative finite difference

scheme,

$$\frac{1}{r_i}\left[\frac{r_{i+\frac{1}{2}}(u_{i+1}-u_i)-r_{i-\frac{1}{2}}(u_i-u_{i-1})}{h^2}\right]=-\frac{G}{\nu}, \qquad i=2,\ldots,n-1, \tag{19}$$

where $r_{i\pm\frac{1}{2}}=r_i\pm\frac{h}{2}$.

At the pipe centreline ($r=0$), regularity of the velocity field requires $\mathrm{d}u/\mathrm{d}r=0$. This condition is enforced numerically by setting

$$u_1=u_2, \tag{20}$$

which corresponds to a second order accurate forward difference approximation to the symmetry condition.

At the pipe wall, the no-slip boundary condition is imposed directly,

$$u_n=0. \tag{21}$$

The resulting systems of linear equations is solved using the same linear solver as in the planar Poiseuille case. The numerical solution is validated by comparison with the analytical velocity profile and the exact expression for the volumetric flow rate.

2.3 Navier slip boundary conditions

Instead of enforcing no slip at solid boundaries, the tangential velocity is allowed to be non zero through the Navier slip boundary condition. This relates the tangential velocity at the wall to the local shear rate via a slip length ℓ, which characterises the degree of slip at the boundary. The no slip condition is recovered in the limit $\ell\to 0$.

2.3.1 Channel flow

For plane parallel pressure driven flow between two plates, the Navier slip condition takes the form

$$l\frac{\partial u}{\partial y}=\pm u \qquad \text{at} \qquad y=\mp W, \tag{22}$$

where the sign accounts for the orientation of the wall normal vector at each boundary.

The governing equation remains

$$-\nu\frac{\mathrm{d}^2u}{\mathrm{d}y^2}=G, \tag{23}$$

but the no slip boundary conditions are replaced by the Navier slip condition above. Solving this equation subject to the slip boundary conditions yields the analytical velocity

profile

$$u(y) = \frac{G}{2\nu}(W^2 - y^2 + 2W\ell). \tag{24}$$

This expression reduces to the classical Poiseuille profile in the limit $\ell = 0$, while increasing values of ℓ lead to an overall increase in the velocity throughout the channel.

In the numerical implementation, the slip boundary condition is enforced using a first order one-sided finite difference approximation to the velocity gradient at the walls. At $y = -W$ and $y = W$, this leads to Robin-type boundary conditions [**?**] which replace the Dirichlet no slip constraints previously used. The resulting system is again tridiagonal and is solved using the same approach as the no slip case.

The analytical solution above provides a direct means of validating the numerical implementation of slip boundary conditions in channel flow.

2.3.2 Axisymmetric Pipe flow

For pressure driven flow in a circular pipe, the Navier slip boundary condition is applied at the pipe wall,

$$\ell\frac{\partial v_z}{\partial r} = -v_z \qquad \text{at } r = R, \tag{25}$$

where $v_z(r)$ is the axial velocity and ℓ is the slip length. As in the channel flow case, the no slip condition is recovered in the limit $\ell \to 0$.

The governing equation for steady axisymmetric flow remains

$$\frac{1}{r}\frac{\mathrm{d}}{\mathrm{d}r}\left(r\frac{\mathrm{d}v_z}{\mathrm{d}r}\right) = -\frac{G}{\nu}, \tag{26}$$

together with the regularity condition $\mathrm{d}v_z/\mathrm{d}r = 0$ at the pipe centreline $r = 0$.

Solving subject to the Navier slip condition yields the analytical velocity profile

$$v_z(r) = \frac{G}{4\nu}(R^2 - r^2 + 2R\ell), \tag{27}$$

which reduces to the classical Poiseuille solution in the absence of slip.

The corresponding volumetric flow rate is

$$\frac{\pi G}{8\nu}(R^4 + 4R^3\ell), \tag{28}$$

demonstrating that slip leads to an enhancement of the flux relative to the no slip case.

It is convenient to express the effect of slip in terms of a normalised flux enhancement,

$$\frac{Q(\ell)}{Q(0)} = 1 + 4\frac{\ell}{R}, \tag{29}$$

which shows that the increase in flow rate scales linearly with the ratio of slip length to

the pipe radius. This dimensionless form provides a direct measure of the influence of Navier slip on global transport properties and is used in section 3 to assess the numerical results.

In the numerical implementation, the slip condition is enforced at the pipe wall using a first order backward finite difference approximation to the radial velocity gradient, replacing the no slip boundary condition previously used.

2.3.3 Shear dependent slip boundary condition for pipe flow

The linear Navier slip condition assumes that the slip length is a constant material parameter, independent of the local flow conditions. Molecular dynamics simulations, however, indicate that the degree of slip can depend on the wall shear rate, particularly at high shear [3]. Thompson and Troian proposed a generalised slip model in which the effective slip length increases with local shear rate and diverges ad a critical value is approached.

In this model, the slip length is given by

$$\ell(\dot{\gamma}_w) = \frac{\ell_0}{\sqrt{1 - \dot{\gamma}_w/\dot{\gamma}_c}}, \tag{30}$$

where ℓ_0 is the low shear (Navier) slip length, $\dot{\gamma}_w$ is the wall shear rate, and $\dot{\gamma}_c$ is a critical shear rate determined by interfacial properties.

For steady axisymmetric pipe flow with axial velocity $v_z(r)$, the wall shear rate is

$$\dot{\gamma}_w = -\frac{\partial v_z}{\partial r}|_{r=R}, \tag{31}$$

where R is the pipe radius. Substituting this expression into the generalised slip model, the Navier slip boundary condition at the pipe wall,

$$v_z(R) = \ell\, \dot{\gamma}_w, \tag{32}$$

is replaced by the non-linear boundary condition

$$v_z(R) = \ell(\dot{\gamma}_w)\, \dot{\gamma}_w = \frac{\ell_0\, \dot{\gamma}_w}{\sqrt{1 - \dot{\gamma}_w/\dot{\gamma}_c}}. \tag{33}$$

In the limit $\dot{\gamma}_w \ll \dot{\gamma}_c$ the effective slip length reduces to $\ell \approx \ell_0$ and the classical Navier slip condition is recovered. This provides a consistent extension of the linear slip model while retaining compatibility with the low shear regime considered elsewhere in this report.

3 Results and discussion

In this section, the numerical schemes developed in section 2 are validated against known analytical solutions for pressure driven channel and pipe flow. Once validated, the effect of Navier slip boundary conditions on the velocity and volume flux is examined.

3.1 Channel flow validation

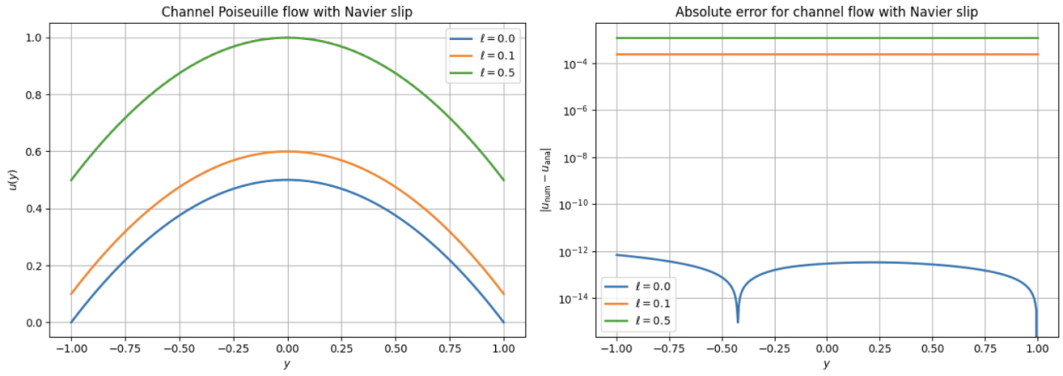

Figure 1: Channel Poiseuille flow with Navier slip. Left: numerical velocity profiles for different slip lengths. Right: absolute error between the numerical and analytical solutions. Colours correspond to different slip lengths.

Figure 1 shows the numerical velocity profiles obtained for pressure driven channel flow with increasing slip length, together with the corresponding absolute errors relative to the analytical solutions. In the no slip case ($\ell = 0$), the numerical solution reproduces the classical parabolic Poiseuille profile with errors at the level of machine precision. This reflects that the second order finite difference scheme exactly captures the quadratic analytical solution.

Introducing Navier slip leads to a non zero velocity at the channel walls and a uniform upward shift of the velocity profile. This is in agreement with the analytical expression derived in section 2. For non zero slip lengths, the error is significantly larger but remains spatially uniform across the domain. This behaviour is expected, as the dominant contribution to the error arises from the first order one sided discretisation of the slip boundary conditions at the walls, limiting the global accuracy of the scheme.

Overall, the close agreement between numerical and analytical solutions confirms the correct implementation of both the finite difference discretisation and the Navier slip boundary condition for channel flow. The same approach is now applied to validate axisymmetric pipe flow.

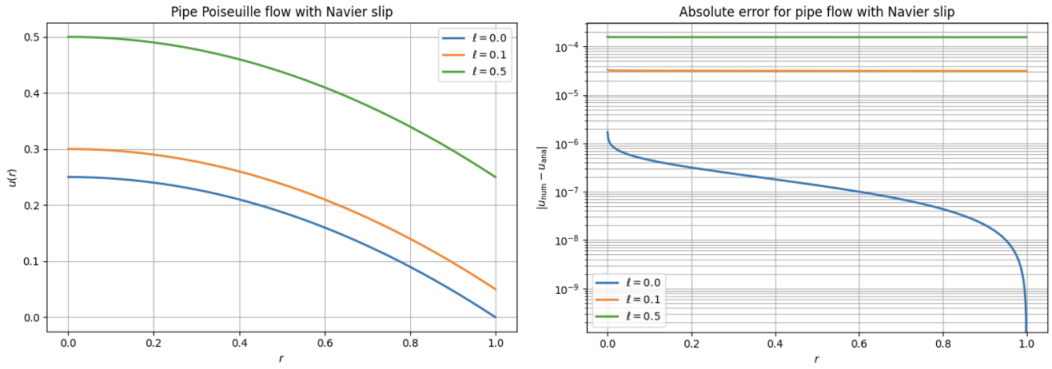

Figure 2: Pipe Poiseuille flow with Navier slip. Left: numerical axial velocity profiles for different slip lengths. Right: absolute error between the numerical solutions and the corresponding analytical profiles. Colours correspond to different slip lengths.

3.2 Pipe flow validation

Figure 2 shows the numerical solutions obtained for pressure driven axisymmetric pipe flow with increasing slip length, together with the corresponding absolute errors relative to the analytical solutions. In the no slip case ($\ell = 0$), the numerical velocity profile reproduces the classical Poiseuille solution. This confirms the correct implementation of the axisymmetric finite difference operator and the symmetry condition imposed at the pipe centreline.

As in the channel flow case, introducing Navier slip leads to a non zero axial velocity at the pipe wall and an increase in the overall magnitude of the velocity profile. In the no slip case ($\ell = 0$), the error exhibits a characteristic radial dependence. It is largest near the pipe centreline, where the axisymmetric operator requires special treatment to enforce regularity, and decreases smoothly across the interior of the domain. The error vanishes sharply at the wall, since the no slip condition is enforced exactly and is satisfied by the analytical solution.

For non zero slip lengths, the dominant contribution to the error instead arises from the first order discretisation of the Navier slip boundary condition at the wall. This introduces a small global offset in the numerical solution, resulting in a larger but spatially smooth error distribution across the radial domain.

Having validated the numerical approach for both channel and pipe geometries, the effect of slip on the volume flux is examined in the following section.

3.3 Volume flux validation

Figure 3 shows the enhancement of the volumetric flow rate with increasing slip length for pressure driven pipe flow. The flux is normalised by the no slip value, allowing the relative effect of Navier slip to be quantified independently of the absolute flow rate. The numerical results are in excellent agreement with the analytical prediction, confirming the solver

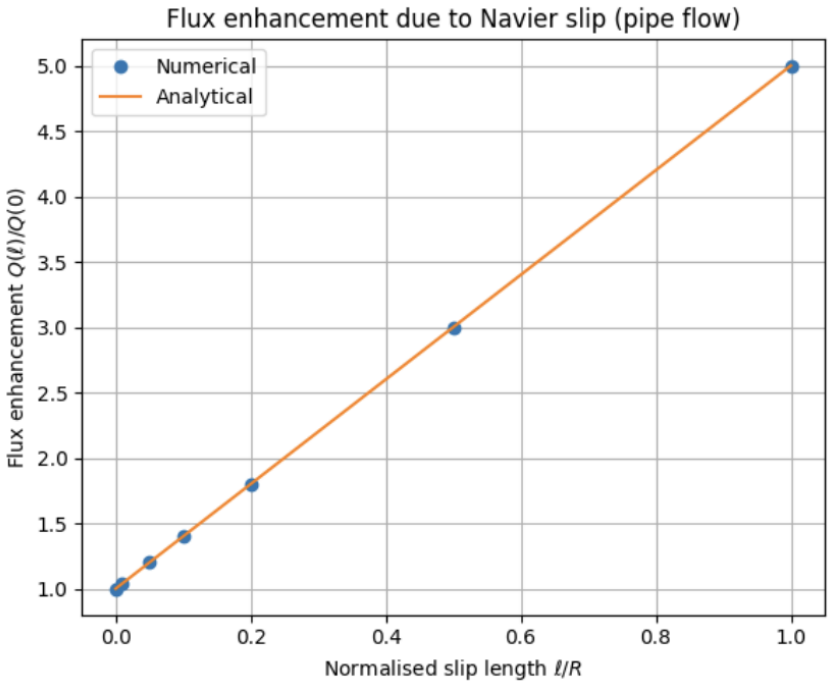

Figure 3: Enhancement of the volumetric flow rate due to Navier slip for pressure-driven pipe flow. The flux is normalised by the no-slip value $Q(0)$ and plotted as a function of the normalised slip length ℓ/R. Symbols denote numerical results and the solid line shows the analytical prediction.

accurately captures the effect of slip on global transport properties. In particular, the linear dependence of the normalised flux enhancement on the slip length is reproduced by the numerical solutions across the full range of slip lengths considered. This demonstrates that the local modification of the boundary condition due to Navier slip leads directly to a proportional increase in the volumetric flow rate.

Overall, these results highlight the sensitivity of pressure-driven viscous flows to boundary conditions and show that even modest slip lengths can result in significant enhancements of transport in confined geometries.

4 Conclusion

In this report, pressure driven viscous flow in channel and pipe geometries has been investigated under both no slip and slip boundary conditions. Analytical solutions for steady Poiseuille flow were derived and used as benchmarks to validate finite difference solvers for the incompressible Stokes equations. In the absence of slip, the numerical solutions reproduce the classical parabolic velocity profiles with errors at the level of machine precision, confirming the correct implementation of the governing equations and boundary conditions.

The introduction of Navier slip leads to a non zero velocity at solid boundaries and

a uniform increase in the magnitude of the velocity profile for both channel and pipe flow. Numerical results were shown to be in excellent agreement with the corresponding analytical solutions. For non zero slip lengths, the dominant contribution to the numerical error arises from the first order discretisation of the slip boundary condition at the wall, resulting in a spatially smooth error distribution while the interior solution remains well resolved.

The effect of slip on global transport was quantified through the volumetric flow rate. In both geometries, slip leads to a significant enhancement of the flux relative to the no slip case. For pipe flow, the numerical results reproduce the analytically predicted linear dependence of the normalised flux enhancement on the slip length, demonstrating that local modifications of the boundary condition translate directly into increased global transport.

Finally, the framework was extended to derive a shear dependent slip boundary condition for pipe flow based on the model of Thompson and Troian [3]. This generalised boundary condition provides a consistent non-linear extension of the Navier slip model and reduces to the classical linear form in the low shear limit. Although not explored numerically in detail, this extension highlights the potential importance of non-linear slip effects at high shear rates and illustrates how microscopic interfacial physics can be incorporated into continuum descriptions.

Overall, this work demonstrates the sensitivity of viscous flows to boundary conditions and highlights the role of slip in modifying both local flow structure and global transport properties in confined geometries.

References

[1] Eric Lauga, Michael P. Brenner, and Howard A. Stone. Microfluidics: The no-slip boundary condition. In Cameron Tropea, Alexander Yarin, and John F. Foss, editors, *Springer Handbook of Experimental Fluid Mechanics*, pages 1219–1240. Springer, 2007.

[2] Michael Whitby, Ludovic Cagnon, Myrto Thanou, and Nick Quirke. Enhanced fluid flow through nanoscale carbon pipes. *Nano Letters*, 8(9):2632–2637, 2008.

[3] P. A. Thompson and S. M. Troian. A general boundary condition for liquid flow at solid surfaces. *Nature*, 389:360–362, 1997.